AFRL-RX-WP-TP-2010-4048

NEXT GENERATION 3D MIXED MODE FRACTURE PROPAGATION THEORY INCLUDING HCF-LCF INTERACTION (PREPRINT)

Richard Pettit, Balkrishna Annigeri, and William Owen

Pratt & Whitney Aircraft

Paul Wawrzynek

Fracture Analysis Consultants

JANUARY 2010

STINFO COPY

**AIR FORCE RESEARCH LABORATORY
MATERIALS AND MANUFACTURING DIRECTORATE
WRIGHT-PATTERSON AIR FORCE BASE, OH 45433-7750
AIR FORCE MATERIEL COMMAND
UNITED STATES AIR FORCE**

REPORT DOCUMENTATION PAGE		*Form Approved* *OMB No. 0704-0188*

1. REPORT DATE *(DD-MM-YY)*	2. REPORT TYPE	3. DATES COVERED *(From - To)*
January 2010	Journal Article Preprint	01 January 2010 – 31 January 2010

4. TITLE AND SUBTITLE

NEXT GENERATION 3D MIXED MODE FRACTURE PROPAGATION THEORY INCLUDING HCF-LCF INTERACTION (PREPRINT)

5a. CONTRACT NUMBER
FA8650-04-C-5200

5b. GRANT NUMBER

5c. PROGRAM ELEMENT NUMBER
62102F

6. AUTHOR(S)

Richard Pettit, Balkrishna Annigeri, and William Owen (Pratt & Whitney Aircraft)
Paul Wawrzynek (Fracture Analysis Consultants)

5d. PROJECT NUMBER
4347

5e. TASK NUMBER
RG

5f. WORK UNIT NUMBER
M02R3000

7. PERFORMING ORGANIZATION NAME(S) AND ADDRESS(ES)

Pratt & Whitney Aircraft
400 Main Street
East Hartford, CT 06108

Fracture Analysis Consultants
121 Eastern Heights Drive
Ithaca, NY 14850

8. PERFORMING ORGANIZATION REPORT NUMBER

9. SPONSORING/MONITORING AGENCY NAME(S) AND ADDRESS(ES)

Air Force Research Laboratory
Materials and Manufacturing Directorate
Wright-Patterson Air Force Base, OH 45433-7750
Air Force Materiel Command
United States Air Force

10. SPONSORING/MONITORING AGENCY ACRONYM(S)
AFRL/RXLMN

11. SPONSORING/MONITORING AGENCY REPORT NUMBER(S)
AFRL-RX-WP-TP-2010-4048

12. DISTRIBUTION/AVAILABILITY STATEMENT
Approved for public release; distribution unlimited.

13. SUPPLEMENTARY NOTES

14. ABSTRACT
The damage tolerance assessment of complex aerospace structural components requires the capability of effective modeling of 3D cracks and their associated propagation and velocity and path under fatigue loads. A 3D mixed mode crack propagation theory is presented which includes the effect of KI, KII, and KIII, as well as non-proportional loading, elastic and fracture resistance anisotropy, and fracture mode asymmetry (viz. the ability to transition between competing tensile and shear modes of propagation). A modified strain energy release rate criterion including the modeling of crack closure is developed and presented for a representative problem. An elementary, mode I characterization of closure is used, leaving shear mode closure as fertile ground for further study. Use of the model is presented for an example problem with steady-vibratory interaction.

15. SUBJECT TERMS
damage tolerance, 3D cracks, propagation, velocity

16. SECURITY CLASSIFICATION OF:			17. LIMITATION OF ABSTRACT:	18. NUMBER OF PAGES	19a. NAME OF RESPONSIBLE PERSON (Monitor)
a. REPORT Unclassified	**b. ABSTRACT** Unclassified	**c. THIS PAGE** Unclassified	SAR	26	Reji John **19b. TELEPHONE NUMBER** *(Include Area Code)* N/A

Standard Form 298 (Rev. 8-98)
Prescribed by ANSI Std. Z39-18

Next Generation 3D Mixed Mode Fracture Propagation Theory including HCF-LCF Interaction

Richard Pettit*, Balkrishna Annigeri*, William Owen*, Paul Wawrzynek**

* Pratt & Whitney Aircraft, 400 Main Street, East Hartford CT 06108

** Fracture Analysis Consultants
121 Eastern Heights Drive, Ithaca, NY 14850

ABSTRACT

The damage tolerance assessment of complex aerospace structural components requires the capability of effective modeling of 3D cracks and their associated propagation and velocity and path under fatigue loads. A 3D mixed mode crack propagation theory is presented which includes the effect of K_I, K_{II}, and K_{III}, as well as non-proportional loading, elastic and fracture resistance anisotropy, and fracture mode asymmetry (viz. the ability to transition between competing tensile and shear modes of propagation). A modified strain energy release rate criterion including the modeling of crack closure is developed and presented for a representative problem. An elementary, mode I characterization of closure is used, leaving shear mode closure as fertile ground for further study.

Use of the model is presented for an example problem with steady-vibratory interaction.

INTRODUCTION

Three-dimensional fracture simulation has advanced significantly over the last few decades. Early work was focused on building the framework to appropriately represent cracks in complex geometries, and calculate sufficiently accurate mixed-mode stress intensity factors [1]. As crack propagation capability followed, much of the effort went to the development of the framework necessary to model the extending crack with minimal user workload, such as the FRANC3D code developed at Cornell University [2]. Non-planar crack growth algorithms typically utilized two-dimensional mode I/II crack turning theories that were well established a generation earlier.

This approach has worked well with a wide range of engineering applications. However, as the technology to model non-planar cracks in complex geometries has matured, the problem set has become more demanding, requiring propagation criteria that include such

things as HCF/LCF interaction, Mixed Non-Proportional Loading (MNPL), fracture mode asymmetry, and both elastic and fracture resistance anisotropy.

Legacy crack propagation/turning criteria, such as the Maximum Tangential Stress (MTS) criterion [3], assume proportional loading (K_{II}/K_I = constant), and predict crack growth along $K_{II} \approx 0$ path. For non-proportional loading, the relative proportions of K_I, K_{II}, and K_{III} vary with time throughout the cycle, and there is no path that enforces $K_{II}=0$ during the entire cycle (not to mention the influence of mode III).   Though widely neglected, MNPL can result from any structural situation wherein steady and cyclic stresses are misaligned, as in the vibrating blade problem illustrated in Figure 1 Vibrating Rotor Blade Resulting in MNPL .
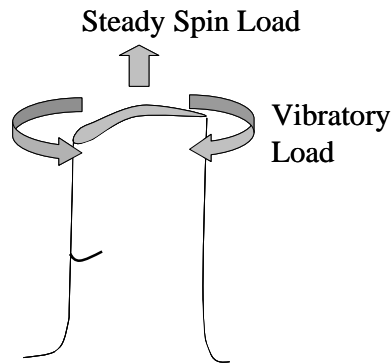
Figure 1 Vibrating Rotor Blade Resulting in MNPL

In order to enable crack growth simulation for this class of problems, two significant advances were required.
1. A validated theoretical approach to handle crack growth and trajectory under MNPL loading.
2. A reduced-order nonlinear dynamics approach to enable FEM vibration modeling including contact between opposing crack faces.

The current paper will deal exclusively with the first of these requirements, though promising approaches to the second problem are a separate subject of investigation [4]. Theoretical enhancements have been implemented in the FRANC3D code as described herein.

Theoretical Background for Crack Growth with Mixed Non-Proportional Loading Conditions

Maximum Stress Criteria
Resolving the (isotropic) lead crack stress intensities, (K_I, K_{II}, K_{III}), into the asymptotic stress intensities (k_I, k_{II}, k_{III}) associated with an infinitesimal crack branch at angle $\Delta\theta$, we obtain

$$k_I(\Delta\theta) = \sigma_{\theta\theta}\sqrt{2\pi r} = \cos\frac{\Delta\theta}{2}\left[K_I\cos^2\frac{\Delta\theta}{2} - \frac{3}{2}K_{II}\sin\Delta\theta\right]$$

$$k_{II}(\Delta\theta) = \sigma_{r\theta}\sqrt{2\pi r} = \frac{1}{2}\cos\frac{\Delta\theta}{2}\left[K_I\sin\Delta\theta + K_{II}(3\cos\Delta\theta - 1)\right] \qquad (1)$$

$$k_{III}(\Delta\theta) = \sigma_{\theta z}\sqrt{2\pi r} = K_{III}\cos\frac{\Delta\theta}{2}$$

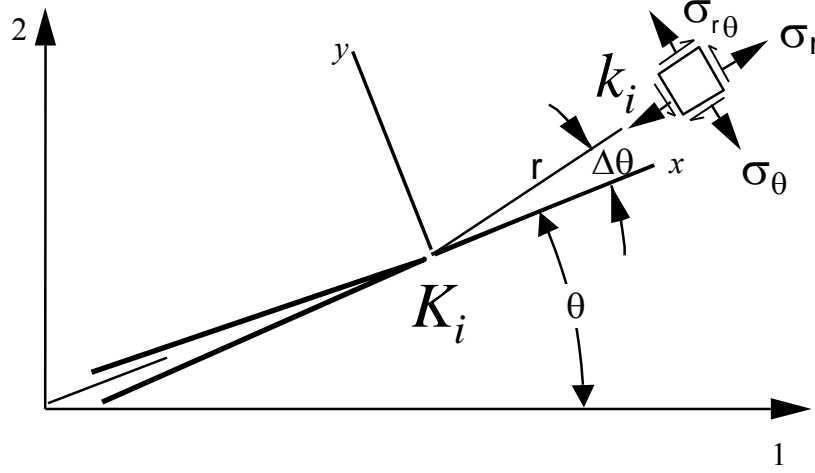For the coordinate system illustrated in Figure 2

Figure 2 Reference coordinate system for theoretical development

A similar solution for 3D anisotropy based on the work of Hoenig [5], will not be further discussed here, but has been be treated and implemented in FRANC3D in much the same manner as the isotropic theory that will now be further discussed.

For proportional loading, the classical Maximum Tangential Stress (MTS) theory, proposed by Erdogan and Sih [2] for isotropic materials, asserts that the crack will grow toward the location of the maximum tangential tensile stress (equivalent to maximizing k_I). By differentiating k_I and equating to zero

$$\frac{K_{II}}{K_I} = \frac{-\sin\Delta\theta_c}{(3\cos\Delta\theta_c - 1)} \qquad (2)$$

or [6]

$$\Delta\theta_c = 2\tan^{-1}\left(\frac{1 - \sqrt{1 + 8(K_{II}/K_I)^2}}{4(K_{II}/K_I)}\right) \qquad (3)$$

where $\Delta\theta_c$ is the kink angle. This criterion seeks out a mode I crack path. As illustrated in Figure 3, the maximum tangential stress theory works well for low ductility materials like PMMA, but fails to predict a transition, observed for 7075-T6 and 2024-T3 aluminum alloys, to a path that is associated with the Maximum Shear Stress (MSS) . In

these materials, the transition is sudden, and the crack seems exclusively dominated by either mode I or mode II.

While it should be noted that the data in Figure 3 is for cracks loaded quasi-statically until the crack begins to tear, as opposed to cyclic loading, similar behavior can occur as a result of cyclic loading, as will be shown.
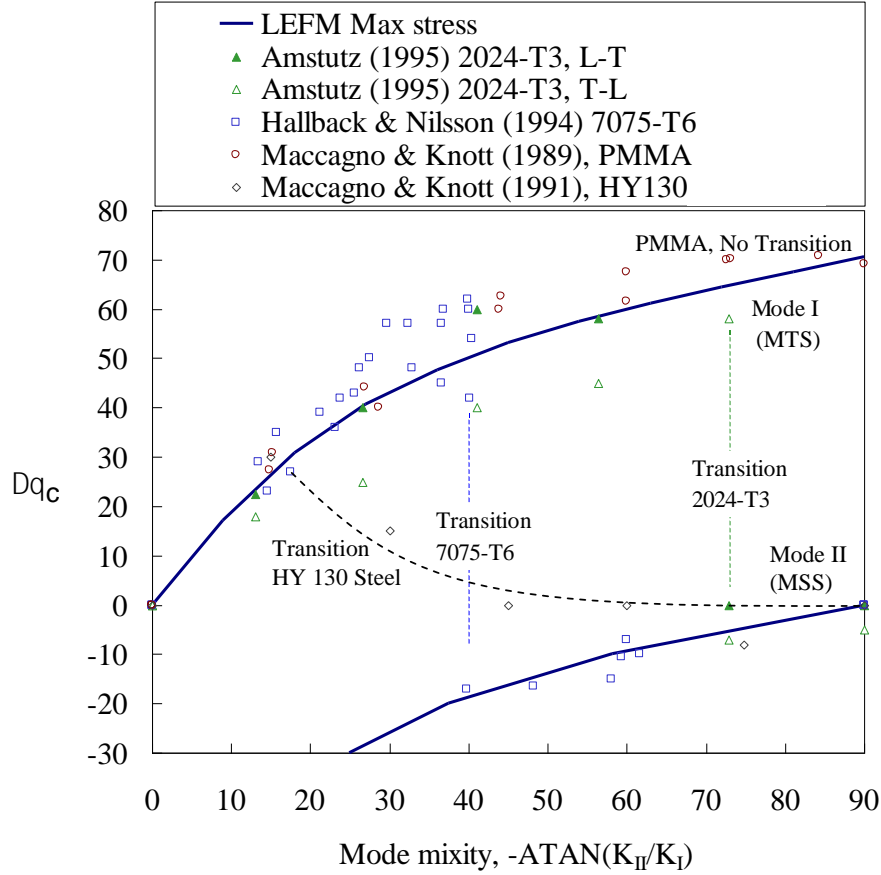

Figure 3 Test data of various investigators [7, 8, 9, 10], showing transition to shear mode dominated growth for ductile metals at high mode mixities

Fracture Mode Interaction and Asymmetry

Chao and Liu [11] describe the sharp transition behavior as a result of competing failure mechanisms in mode I and mode II as shown in Figure 4. According to their hypothesis, the two modes do not interact (see also [12]), and the crack will fail in Mode I unless

$$\left.\frac{k_I(\Delta\theta)}{K_{IC}}\right|_{max} < \left.\left|\frac{k_{II}(\Delta\theta)}{K_{IIC}}\right|\right|_{max} \quad (4)$$

Where K_{Ic} and K_{IIc} are the pure mode fracture toughness values for a straight growing crack, and the subscript "max" denotes maximizing with respect to the kink angle. For the purpose of further discussion, this criterion will be described as the "Modal" fracture criterion
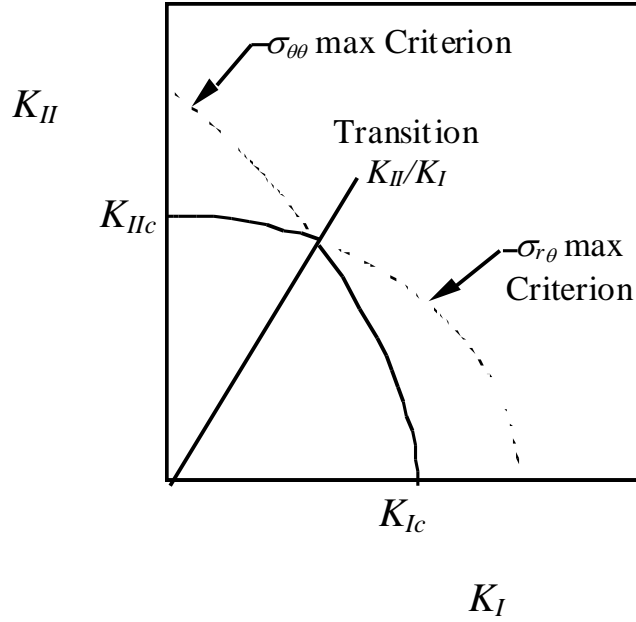
4

Figure 4 Transition mechanism proposed by Chao and Liu {11]

Note, however, that the HY130 steel in Figure 3 behaves in a different manner[1], exhibiting a more gradual transition to a kink angle of zero, rather than the angle associated with maximum mode II. Thus, both tensile and shear modes of growth appear to be contributing to failure. This type of behavior correlates well to a Modified Strain Energy Release Rate (MSERR) approach proposed by Kfouri & Brown [13], that suggests a failure locus of the form

$$\left(\frac{k_I(\Delta\theta)}{K_{IC}}\right)^2 + \left(\frac{k_{II}(\Delta\theta)}{K_{IIC}}\right)^2 = 1 \qquad (5)$$

For a non-critical load state, the most critical crack growth direction would be obtained by maximizing the left hand side of this equation with regard to θ. A measure of how nearly critical the loading is in terms of an equivalent mode I stress intensity can be written by solving Equations (4) and (5) for K_{Ic} respectively and rewriting so that the crack is critical if $k_{Ieq} = K_{IC}$.

$$k_{1eq} = MAX\left\{k_I(\Delta\theta)\big|_{max}, \frac{K_{IC}}{K_{IIC}}\big|k_{II}(\Delta\theta)\big|_{max}\right\} \qquad \text{(Modal)} \qquad (6)$$

$$k_{Ieq} = \sqrt{[k_I(\Delta\theta)]^2 + \left(\frac{K_{IC}}{K_{IIC}}\right)^2 [k_{II}(\Delta\theta)]^2}\;\Big|_{max} \qquad \text{(MSERR)} \quad (7)$$

---

[1] The HY-130 tests exhibited tearing in a zig-zag microscopic shear mode. The crack turning angles shown for this alloy were read from Maccagno and Knott's photographs, and reflect the average trend of the zig-zag line, consistent with our intent. Maccagno and Knott gave quite different values of the turning angle.

While the modal criterion assumes non-interaction of modes I and II, modes II and III are both shear modes, and can be combined into a resolved shear stress intensity

$$k_{23} = \sqrt{k_{II}^2 + k_{III}^2} \qquad (8)$$

It seems reasonable to assume that such modes would interact in materials that fail by either the Modal or MSERR criterion, which infers that equations (6) and (7) can be generalized in 3D to

$$k_{Ieq} = MAX \left\{ k_I \left(\Delta\theta\right)\big|_{max}, \sqrt{\left(\frac{K_{IC}}{K_{IIC}}\right)^2 [k_{II}\left(\Delta\theta\right)]^2 + \left(\frac{K_{IC}}{K_{IIIC}}\right)^2 [k_{III}\left(\Delta\theta\right)]^2} \Bigg|_{max} \right\} \qquad (9)$$

(Modal)
and,

$$k_{Ieq} = \sqrt{[k_I\left(\Delta\theta\right)]^2 + \left(\frac{K_{IC}}{K_{IIC}}\right)^2 [k_{II}\left(\Delta\theta\right)]^2 + \left(\frac{K_{IC}}{K_{IIIC}}\right)^2 [k_{III}\left(\Delta\theta\right)]^2} \Bigg|_{max} \qquad (10)$$

(MSERR)
The ratios K_{IC}/K_{IIC} and K_{IC}/K_{IIIC} are measures of the *fracture mode asymmetry* of a material, a term coined by Kfouri describing the relative fracture resistance of a given material in the different modes. The material dependent transition points observed in the data in Figure 3 can be correlated to different values of these ratios. While the fracture mode asymmetry is couched in terms of fracture toughness ratios, the intent is to view these ratios as material parameters in their own right, that can be used to model the transitions between tensile and shear crack propagation under both monotonic and cyclic loading conditions.

Fracture Resistance Anisotropy
In addition to fracture mode asymmetry, which addresses the relative fracture resistance of a material to the different fracture modes, there is also the potential for the fracture resistance to vary as a function of crack orientation within the material. Buczeck and Herakovitch [14] expressed the fracture resistance in 2D as a simple elliptical function. This was generalized to include a more flexible interpolation function, as shown in Figure 5, and extended to 3D [15, 16, 17] to express the (pure mode) stress intensity factor at which a crack will propagate in an arbitrary orientation. The crack orientation in 3D is identified by the normal and tangential vectors (**n,a**) as illustrated in Figure 6a.
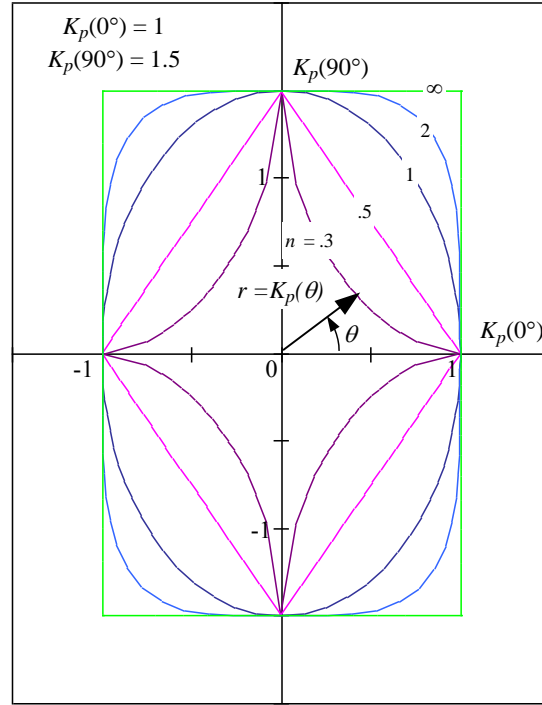
$$K_p(\theta) = \left[\left(\frac{\cos^2 \theta}{K_p(0°)^2} \right)^n + \left(\frac{\sin^2 \theta}{K_p(90°)^2} \right)^n \right]^{-\frac{1}{2n}}$$

Figure 5 Polar interpolation function for fracture resistance anisotropy in 2D [16, 17]
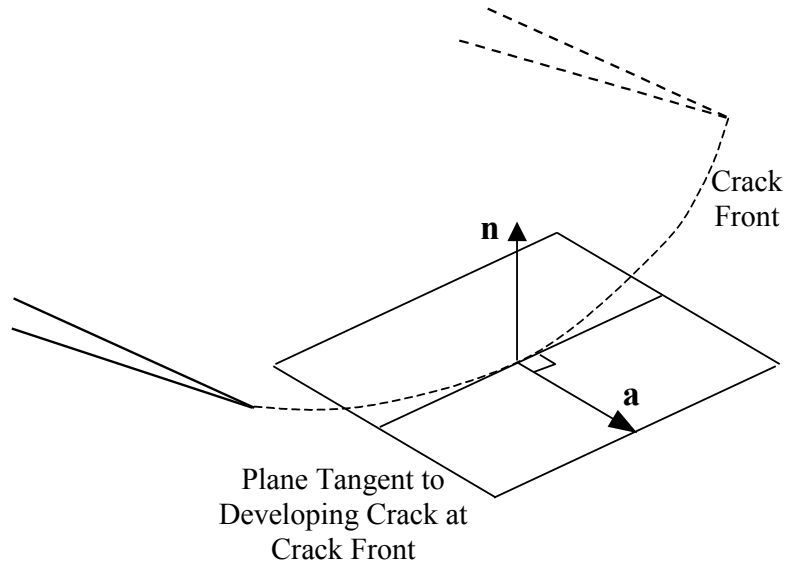
a. Geometry of *crack* orientation at a point on an arbitrary crack front

b. Principle fracture resistance values and traces of crack growth direction **a** in cardinal planes

Figure 6 Physical Parameters Governing 3D Fracture Resistance Anisotropy [15]

Assuming three principle planes of material symmetry, each with their own 2D fracture resistance interpolation functions as shown in Figure 6b, the stress intensity at which a crack will propagate in the (**n,a**) orientation is given by

$$K_p(\mathbf{n},\mathbf{a}) = \left[\left(\frac{n_1^2}{K_1^2}\right)^\ell + \left(\frac{n_2^2}{K_2^2}\right)^\ell + \left(\frac{n_3^2}{K_3^2}\right)^\ell\right]^{-\frac{1}{2\ell}} \quad (11)$$

Where the trace fracture resistance values, K_i of the a vector in fracture resistance space, as illustrated in Figure 6b, are given by

$$K_i(\mathbf{a}) = \frac{\sqrt{1-a_i^2}}{\left[\left(\frac{a_j^2}{K_{ij}^2}\right)^m + \left(\frac{a_k^2}{K_{ik}^2}\right)^m\right]^{\frac{1}{2m}}} \qquad \text{(non-repeating)} \quad (12)$$

and the K_{ij} are the six principal fracture resistance values in 3D (two for each principal planes), and n_i and a_i are the components of the n and a vectors. Depending on processing symmetries, the six principal fracture resistance values may not all be unique. If they are all equal, and $\ell m=1$, the properties are isotropic with regard to fracture resistance.

For the purposes of the current development, K_p will be considered to be normalized to the fracture resistance in a reference orientation, likely chosen to be the orientation for which the properties are most fully characterized. By definition, $K_p=1$ in the reference orientation.

Extension to Fatigue Crack Growth
For application to fatigue crack growth, the six principal fracture resistance parameters and the fracture mode asymmetry parameters are assumed to be the same for all crack growth in a given material, whether near threshold or approaching the fracture toughness. This implicitly assumes that, the ΔK^{eff} vs da/dN curves are parallel regardless of crack orientation or modality of failure, and any differences can be represented by an appropriate horizontal shift (in K_{max} and ΔK^{eff}). While this is almost certainly an oversimplification, it represents an attempt to include all these real-world effects in the simplest way possible[2].

When we speak of ΔK^{eff} in this venue, we are referring to the cyclic stress intensity that actually makes it to the crack tip, as opposed to the globally applied ΔK. Among the potential crack tip shielding effects, Mode I plasticity induced crack closure [18], though still a topic of lively discussion, remains an industry standard approach to account for R-ratio effects. Add shear modes, and there is the potential for friction to reduce the effective shear cyclic stress intensity. While there is ample evidence for shear mode crack tip shielding in the literature [19, 20, 21] no quantitative theoretical framework has become widely accepted for modeling this behavior.

Despite these difficulties, it was recognized that without taking into account shielding effects in some way, known phenomena could not be predicted. Also, it was desired to at least maintain industry standard capability for mode I problems, including the ability to predict the effect of R-ratio. It was thus decided to adopt as a baseline the NASGRO crack growth model formulation [22, 23], including the Newman closure equations for

---

[2] Kfouri suggested that the fracture mode asymmetry might also be a function of orientation, but that possibility was excluded in the current formulation.

Mode I closure, and attempt to extend the equations in a rudimentary way to account for mixed modes. While it was recognized that this could potentially have serious shortcomings, it would serve at least as a temporary member in the overall theoretical framework, with the opportunity to improve upon it as better methods become available. For the purposes of the present formulation, we will again invoke the steady-vibratory scenario of Figure 1, and introduce the notation

$$\Delta K = K^{+} - K^{-} \qquad (13)$$

Superscripts refer to the extreme values, max and min, for K_I, and to the corresponding extreme values for the shear modes. That is, the positive sign will correspond to the extreme load state with the most positive K_I value, regardless of the sign or magnitude of the shear modes.

Referring to Figure 3, there are two possible assumptions that could be made with regard to crack closure:

-Closure occurs in the **lead crack** only (no infinitesimal kink, resolved stresses only)
-Closure behavior occurs in the infinitesimal **kink tip**

With the assumption of kink tip closure, crack growth is evaluated at the infinitesimal kink tip, and Eq 13 would written in lower case k's , and be evaluated (and the sign convention established) at the kink tip. While capital (lead crack) notation will be followed on the next few equations, bear in mind that they would be written in lower case (kink tip) notation for the second assumption above. With that in mind, crack closure will be defined by the mode I component.

$$\Delta K_I^{eff} = K_I^{+} - K_I^{op} = \Delta K_I F_1 \qquad (14)$$

Where Newman and global closure options as shown in Figure 7.

$$F_1 = \begin{cases} 0 & if \ K^{+} \le 0 \\ 1 & for \ \Delta k^{applied} \\ f(R) & for \ Newman \ closure \\ \dfrac{\min(K_I^{+}, \Delta K_I)}{\Delta K_I} & for \ global \ closure \end{cases} \qquad (15)$$
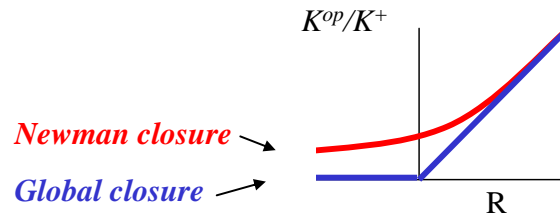

Figure 7 Illustration of Newman and global closure

The Newman closure function (slightly modified by the additional material parameter C for negative R-ratios) is given by

$$f[R] = \frac{\Delta K_I^{eff}}{\Delta K_I} = \frac{\left(1 - S^{op}/S^+\right)}{\left(1 - R\right)}$$

where $\hspace{8cm}$ (16)

$$S^{op}/S^+ = A_o + CA_1 R \hspace{3cm} for \quad -1 \le R < 0$$

$$S^{op}/S^+ = MAX(A_o + A_1 R + A_2 R^2 + A_3 R^3, R) \hspace{1cm} for \quad R \ge 0$$

$$A_o = \left(.825 - .34\alpha + .05\alpha^2\right)\left[\cos\left(\frac{\pi S^+}{2\sigma_o}\right)\right]^{\frac{1}{\alpha}}$$

$$A_1 = \left(.415 - .071\alpha\right)S^+/\sigma_o$$

$$A_2 = 1 - A_o - A_1 - A_3$$

$$A_3 = 2A_o + A_1 - 1$$

$$\alpha = constraint\ factor = \begin{cases} 1.0 & plane\ stress \\ 3.0 & plane\ strain \end{cases}$$

$$\sigma_o = flow\ stress$$

$$R = \frac{K_I^-}{K_I^+}$$

While ΔK_{II} and ΔK_{III} do not "close" in the sense that mode I does, it can first be postulated that once the kink tip closes in mode I, a "stick" or "slip" condition exists, altering ΔK_{II} and ΔK_{III} as follows

$$\Delta K_{II}^{eff} = \Delta K_{II} F_{23}$$

$$\Delta K_{III}^{eff} = \Delta K_{III} F_{23}$$

where $\hspace{5cm}$ (17)

$$F_{23} = \begin{cases} F_1 & for\ stick\ friction \\ 1 & for\ slip\ friction \end{cases}$$

For simple sliding friction, F_{23} should lie between stick and slip values. For (Newman) closure over a small region near the tip of the crack, the weight functions for tension and shear modes are identical, thus the maximum amount of K_{23} that can be dissipated in Coulomb friction by a compressive K_I is

$$K_{23}^{frict} = \mu K_I^{comp} \quad where \quad K_I^{comp} = Max(0, K_I^{op} - K_I) \hspace{1cm} (18)$$

To the degree that the global weight functions for tensile and shear are in agreement, these expressions will also be approximately true for global closure. Allowing the possibility of closure at both extremes of the cycle,

$$F_{23} = Max\left\{1 - \frac{\mu\left[K_I^{comp+} + K_I^{comp-}\right]}{\sqrt{\Delta K_{II}^2 + \Delta K_{III}^2}}, F_1\right\} \quad for\ Coulomb\ friction \hspace{1cm} (19)$$

Note that like the stress intensity factors, the closure parameters F_1 and F_{23} may be written in lower case when they refer to values evaluated at the kink tip.

Lead Crack Closure

The lead crack stress intensity factors and R-ratio for lead crack closure may be expressed as

$$\begin{bmatrix} K_I^{\pm} \\ K_{II}^{\pm} \\ K_{III}^{\pm} \end{bmatrix} = \begin{bmatrix} K_I \\ K_{II} \\ K_{III} \end{bmatrix}_{st} \pm \begin{bmatrix} K_I \\ K_{II} \\ K_{III} \end{bmatrix}_{vib} \qquad (20)$$

$$R_I = \frac{K_I^-}{K_I^+} \qquad (21)$$

The opening stress intensity factors are given by

$$\begin{bmatrix} K_I^{op} \\ K_{II}^{op} \\ K_{III}^{op} \end{bmatrix} = \begin{bmatrix} K_I^+ \\ K_{II}^+ \\ K_{III}^+ \end{bmatrix} - \begin{bmatrix} F_1(K_I^+ - K_I^-) \\ F_{23}(K_{II}^+ - K_{II}^-) \\ F_{23}(K_{III}^+ - K_{III}^-) \end{bmatrix} \qquad (22)$$

In the special case where $K_I^+ < 0$, K_I^+ and K_I^{op} must are set to zero for compression-compression loading. The effective crack tip Δk values are calculated from the lead K^+ and K^{op} values using (1).

$$\begin{bmatrix} \Delta k_I^{eff} \\ \Delta k_{II}^{eff} \\ \Delta k_{III}^{eff} \end{bmatrix} = \begin{bmatrix} k_I^+(\Delta\theta) - k_I^{op}(\Delta\theta) \\ abs[k_{II}^+(\Delta\theta) - k_{II}^{op}(\Delta\theta)] \\ abs[k_{III}^+(\Delta\theta) - k_{III}^{op}(\Delta\theta)] \end{bmatrix} \qquad (23)$$

It is postulated that the crack will grow in the direction corresponding to the maximum growth rate, da/dN, associated with these Δk values, which will require a numerical search to maximize an appropriate growth parameter. Note that the use of resolved $\Delta k_I^{eff}(\Delta\theta)|_{max}$ as the crack turning criterion with global closure, proportional loading, and positive K_I values yields results equivalent to the MTS crack turning criterion. A more general criterion will be proposed later on.

One area of discomfort evident in the foregoing formulation is the treatment of negative R-ratios. In NASGRO and other legacy codes, negative K's are nominally allowed, and act to accelerate the crack growth via negative R-ratios using the Newman closure equations (an approach with its own shortcomings even for mode I loading). In mixed-mode situations, however, allowing negative K_I values (which unrealistically involves crack faces passing through each other) leads to resolved mode II components at non-zero θ. Yet, neglecting negative K_I values neglects the associated acceleration associated with –R ratios.

Kink Tip Closure

The lead crack stress intensity factors needed to evaluate kink tip closure are the same as given in Equation (20), except that for the reasons just discussed, in the case of a negative R-ratio at the lead crack it was found necessary to enforce global closure (truncate negative K_I at zero) on the K_I term before evaluating its contribution to mode II at the kink tip. Negative lead crack K_I's are allowed to contribute to k_I, to preserve the negative R-ratio acceleration for near-mode I scenarios.

Theoretically, the sign convention as to which is the + side of the cycle is not decided until the kink tip stress intensity factors and ranges are calculated from the lead crack values using (1).

$$\begin{bmatrix} \Delta k_I \\ \Delta k_{II} \\ \Delta k_{III} \end{bmatrix} = abs \begin{bmatrix} k_I^+(\Delta\theta) - k_I^-(\Delta\theta) \\ k_{II}^+(\Delta\theta) - k_{II}^-(\Delta\theta) \\ k_{III}^+(\Delta\theta) - k_{III}^-(\Delta\theta) \end{bmatrix} \quad (24)$$

However, by taking the absolute value and by defining the mode I R-ratio as

$$R_I(\Delta\theta) = \frac{MIN(k_I^+, k_I^-)}{MAX(k_I^+, k_I^-)} \quad (25)$$

we rectify the use of the lead crack sign convention (as will be seen, the sign of the shear mode ranges is later squared, and is thus inconsequential). The kink tip effective stress intensity ranges then given by

$$\begin{bmatrix} \Delta k_I^{eff} \\ \Delta k_{II}^{eff} \\ \Delta k_{III}^{eff} \end{bmatrix} = \begin{bmatrix} f_1 \Delta k_I \\ f_{23} \Delta k_{II} \\ f_{23} \Delta k_{III} \end{bmatrix} \quad (26)$$

Generalized Crack Propagation Criteria

As alluded to earlier, determination of the crack growth direction will require a numerical search to maximize an appropriate growth parameter. Following the approach of Buzcek and Herakovitch [14] used successfully in FRANC2D [24] for many years, the crack is postulated to grow in the direction so that the ratio between the crack driving force and the crack growth resistance is maximized.

$$\left\{ \frac{Crack\ driving\ force(\Delta\theta)}{Crack\ growth\ resistence(\Delta\theta)} \right\}_{max} \quad (27)$$

Writing Equations (9, 10) in terms of Δk^{eff} as crack driving forces, and using (11) for the crack growth resistance, we can write the generalized crack propagation criteria as

$$\Delta k_{Ieq}^{eff} = MAX \left\{ \left(\frac{\Delta k_I^{eff}}{K_p} \right)_{max}, \left(\frac{1}{K_p} \sqrt{\left(\frac{K_{IC}}{K_{IIC}} \right)^2 \Delta k_{II}^{eff\,2} + \left(\frac{K_{IC}}{K_{IIIC}} \right)^2 \Delta k_{III}^{eff\,2}} \right)_{max} \right\} \quad (28)$$

(Modal)
And,

$$\Delta k_{Ieq}^{eff} = \left\{ \frac{1}{K_p} \sqrt{\Delta k_I^{eff\,2} + \left(\frac{K_{IC}}{K_{IIC}} \right)^2 \Delta k_{II}^{eff\,2} + \left(\frac{K_{IC}}{K_{IIIC}} \right)^2 \Delta k_{III}^{eff\,2}} \right\}_{max} \quad (29)$$

(MSERR)
Note that these $\Delta k_{I\,eq}^{eff}$ values are *effective* in the sense that they are closure adjusted, and *equivalent* in the sense that they include all mixed mode effects (to the extent the theory is capable), and can thus be used in conjunction with a standard *mode I* closure model. The angle resulting from the maximization, θ_c, is the predicted kink angle.

<u>Use of the NASGRO Equation</u>
The NASGRO Equation for calculation of the crack growth rate is given as follows [22].

$$\frac{da}{dN} = C \ (\Delta k_{eq}^{eff})^b \ \frac{\left(1 - \frac{\Delta K_{th}}{\Delta K_{applied}}\right)^p}{\left(1 - \frac{K_{max}}{K_c}\right)^q} \qquad (30)$$

Where we have taken the liberty of including $\Delta k_{I\,eq}^{eff}$ and,

$$\Delta K_{th} = \begin{cases} \dfrac{\left(\Delta K_1^* f^{-(1+RC_P)}\right)}{\left(1-A_0\right)^{(1-R)C_P}} & for \ R \ge 0 \\[4mm] \dfrac{\left(\Delta K_1^* f^{-(1+RC_N)}\right)}{\left(1-A_0\right)^{(C_P-RC_N)}} & for \ R < 0 \end{cases} \qquad (31)$$

$$\Delta K_1^* = \Delta K_1 \sqrt{\left(\frac{a}{a+a_0}\right)} \quad (32)$$

$$K_C = K_{IC}\left(1 + B_k e^{-\left(\frac{A_k t}{t_0}\right)^2}\right) \quad where \ t_0 = 2.5\left(\frac{K_{IC}}{\sigma_{ys}}\right) \qquad (33)$$

The problem is that K_{max} and $\Delta K_{applied}$, as required in Equation (30), are not defined in a manner sufficiently general to include mixed mode behavior. It is proposed that K_{max} be generalized by using the equivalent value.

$$k_{I\,eq}^{max} = MAX\left\{k_{I\,eq}^+, k_{I\,eq}^-\right\} \qquad (34)$$

Where $\Delta k_{I\,eq}$ can be written for the two material behaviors as

$$k_{I\,eq} = MAX\left\{\left(\frac{k_I}{\overline{K}_p}\right)_{\Delta\theta=\Delta\theta_c}, \left(\frac{1}{\overline{K}_p}\sqrt{\left(\frac{K_{IC}}{K_{IIC}}\right)^2 k_{II}^2 + \left(\frac{K_{IC}}{K_{IIIC}}\right)^2 k_{III}^2}\right)_{\Delta\theta=\Delta\theta_c}\right\} \qquad (35)$$

(Modal)
and,

$$k_{I\,eq} = \left\{\frac{1}{\overline{K}_p}\sqrt{k_I^2 + \left(\frac{K_{IC}}{K_{IIC}}\right)^2 k_{II}^2 + \left(\frac{K_{IC}}{K_{IIIC}}\right)^2 k_{III}^2}\right\}_{\Delta\theta=\Delta\theta_c} \qquad (MSERR) \quad (36)$$

The $\Delta K_{applied}$ value to be used to shape the near-threshold regime is more difficult to define with confidence, in part, because there is some evidence [25] that as threshold is approached (very small scale yielding), the modal transition sometimes disappears (suggesting that the fracture mode asymmetry ratios reduce near threshold). Based on this tentative observation, one might simply assume that ΔK_{th} in Equation (30) is evaluated using (31) with R= R_I, and use Δk_I (calculated with no closure, thus the same as in (24)) as $\Delta K_{applied}$. However, this would require that θ_c be determined by maximizing (30) instead of (28) or (29). Such an approach might have merit, driving cracks in a mode I direction near threshold, but could potentially be non-conservative if shear modes

were able to contribute to propagation in the near-threshold regime. On the other hand, one could conservatively neglect threshold altogether.

For the current implementation it was decided to calculate pure mode thresholds as follows.

$$\Delta K_I^{th} = \begin{smallmatrix} Calculated\ per\ NASGRO \\ model\ with\ R=R_I \end{smallmatrix}$$

$$\Delta K_{II}^{th} = \frac{K_{IIc}}{K_{Ic}} \Delta K_1^* \qquad (37)$$

$$\Delta K_{III}^{th} = \frac{K_{IIIc}}{K_{Ic}} \Delta K_1^*$$

The use of the intrinsic (closure-free) thresholds as the basis for estimating shear mode threshold is almost certainly conservative. The equivalent applied values may then be calculated.

$$k_{I\,eq}^{applied} = CRIT \left\{ \left(\frac{\Delta k_I^{applied}}{\overline{K}_p} \right)_{\Delta\theta=\Delta\theta_c}, \left(\frac{1}{\overline{K}_p} \sqrt{ \left(\frac{\Delta K_I^{th}}{\Delta K_{II}^{th}} \right)^2 k_{II}^{applied2} + \left(\frac{\Delta K_I^{th}}{\Delta K_{III}^{th}} \right)^2 k_{III}^{applied2} } \right)_{\Delta\theta=\Delta\theta_c} \right\}$$

(modal)   (38)

$$k_{I\,eq}^{applied} = \left\{ \frac{1}{\overline{K}_p} \sqrt{ \Delta k_I^{applied2} + \left(\frac{\Delta K_I^{th}}{\Delta K_{II}^{th}} \right)^2 \Delta k_{II}^{applied2} + \left(\frac{\Delta K_I^{th}}{\Delta K_{III}^{th}} \right)^2 \Delta k_{III}^{applied2} } \right\}_{\Delta\theta=\Delta\theta_c}$$

(MSERR)   (39)

ΔK_I^{th} and $\Delta k_{I\,eq}^{applied}$ are substituted for Δk_{th} and $\Delta k_{applied}$ in Equation (30) to calculate the crack growth rate. This method is not expected to perform well at predicting MPNL threshold behavior, but should serve as a lower bound for the purposes of crack growth analyses until a better method becomes available.

Correlation with Tension-Torsion Data

A mixed mode/non-proportional loading test program was undertaken to provide MNPL crack turning data. Specimens were made of IN718 nickel alloy, machined into a tension-torsion configuration with through-wall cracks, and thus were predominantly loaded in mode I/II. Tests included specimens with tension and torsion loading in-phase, tension constant and cyclic torsion, torsion constant and cyclic tension, and tension and torsion loading180 degrees out-of-phase. Fabrication and testing took place at NASA MSFC, and fractography and K-solution development was performed by Shelby Highsmith [26] at Georgia Tech. A summary of the test data is provided in Table 1. Some crack tips were observed to bifurcate initially, with one of the kinks subsequently becoming dominant. In other cases, a negative kink would occur on one crack tip, and a positive kink on the other (speaking in crack tip coordinates, so a "symmetric" looking kink arrangement is actually one positive and one negative). In all these cases, both primary and secondary angles were recorded (though it wasn't always clear which was

15

which), and when more than one like angle resulted, they were averaged in the table. For further detail, see [26].

Table 1. Inco 718 Crack Kink angle Data

	Spec No	RI	RII	RIII	KI+	KII+	KIII+	Mean Beq	Measured Kink Angles Primary	Secondary
In Phase	1	0.6	0.6	0.6	19.160	10.280	5.6100	28.22	-37.0	
	2	0.6	0.6	0.6	19.435	10.670	5.7000	28.77	-37.0	
	8	0.1	0.1	0.1	10.940	10.830	2.1700	44.71	-38.0	**8.5**
	9	0.1	0.1	0.1	11.025	10.725	2.7600	44.21	-56.5	**17**
	12	0.1	0.1	0.1	16.470	7.170	1.7200	23.53	-28.0	
	16	0.1	0.1	0.1	13.600	8.850	2.3800	33.05	-32.5	
KI Const	3	1	0.6	0.6	17.705	11.090	3.2300	26.33	-54.5	
	4	1	-1	-1	17.775	11.175	2.5200	0.00	**0.0**	
	6	1	0.0204	0.0204	20.405	10.430	6.3750	13.84	**4.5**	
	10	1	0.1	0.1	10.445	10.365	2.2000	25.22	**1.0**	
	13	1	0.1	0.1	16.130	7.195	1.0650	13.30	-46.5	**5.5**
KII Const	5	0.6	1	1	21.470	10.755	7.0400	33.23	-16.0	
	7	0.1	1	1	15.480	15.470	2.4250	64.63	-15.5	
	11	0.1	1	1	16.240	6.970	1.9600	50.06	-10.5	
Out of Phase	17	0.1	10	10	14.130	0.902	0.2770	42.37	-38.0	
	18	0.1	10	10	9.960	0.964	0.2770	44.81	-64.0	**6.0**
	19	0.1	10	10	16.075	0.691	0.1965	39.68	**14.5**	

The data was fit to an MNPL model that captured modal transition behavior and other trends quite well, except possibly for the out-of-phase data. Observed crack turning angles show excellent correlation with the model, as presented in Figure 8. Hollow symbols represent model predictions, and (neighboring) solid symbols are test data, with both primary and secondary angles plotted. Note that Highsmith defined the experiments with shear of opposite sign to the data in Figure 3, resulting in "flipped" plots.
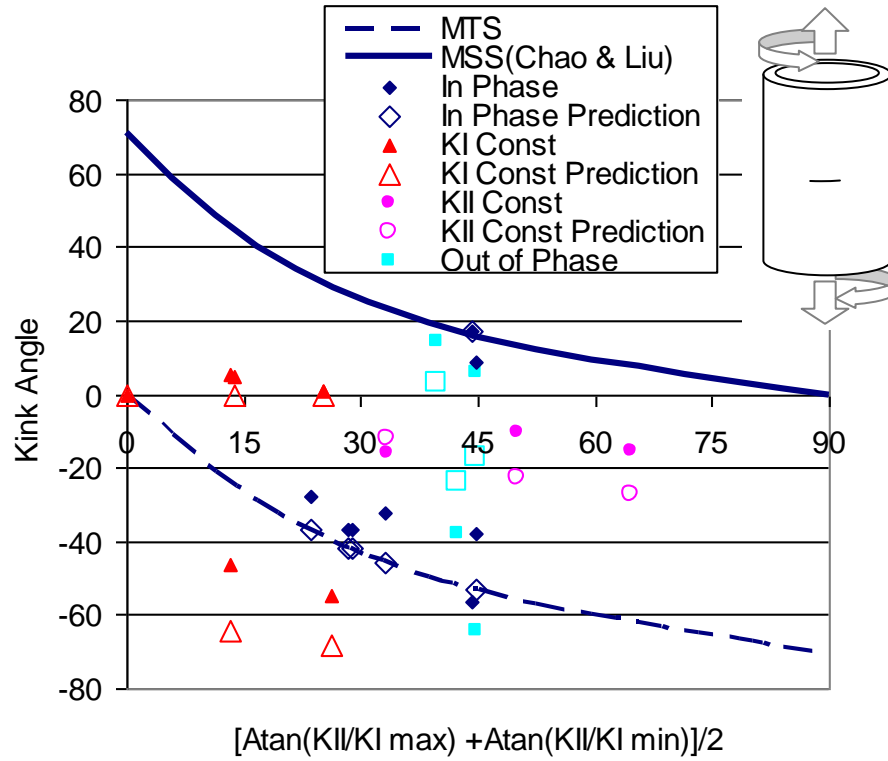
Figure 2.2 Correlation of Mixed-Mode, Non-Proportionally Loaded Specimens Data with Predicted Kink Angles

The ability to correlate the data was encouraging, and fracture surface examination (Figures 2.2a and 2.2b) showed a striking difference in appearance for tensile and shear dominated fracture, lending additional credibility to the existence of a fracture mode transition. On the down side, it was found that the data could be fit fairly comparably using more than one combination of parameters, which would predict significantly different growth rates. Unfortunately, crack growth rates were not measured during these tests, so a unique best fit could not be established for lifing purposes.
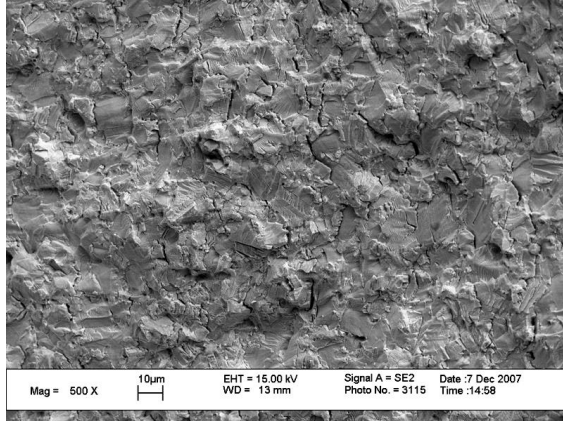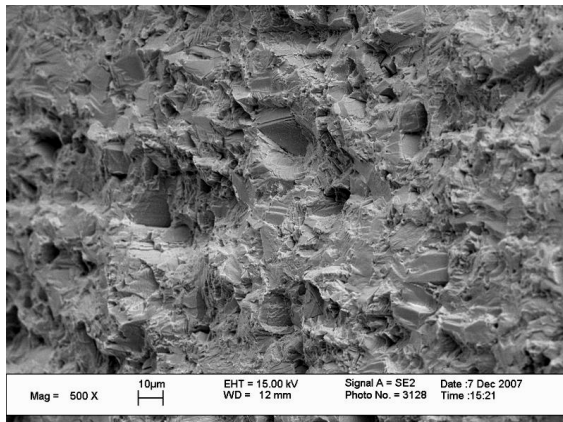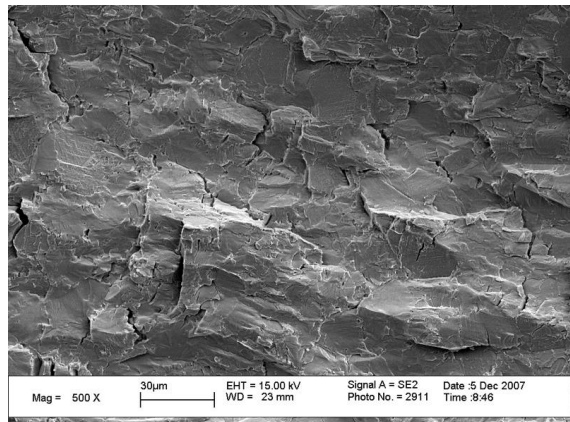
Tensile crack (MHS) deflection
$\theta = -27°$
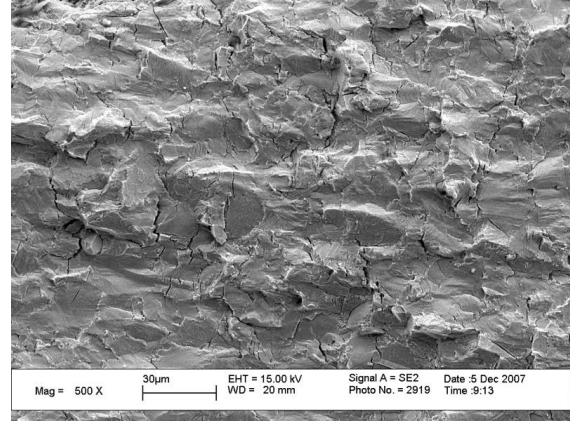
Shear crack (MSS) deflection
$\theta = 18°$

a. In-phase

Tensile crack (MHS) deflection
$\theta = -41°$

Shear crack (MSS) deflection
$\theta = 1°$

b. Constant tension/cyclic torsion

Figure 2.3 Crack Face Appearance for Tensile and Shear Dominated Crack Growth [28]

Discussion

An implementation of an MNPL crack growth approach has been presented capable of analyzing a constant amplitude linear cycle between two points. While this is an encouraging advance, significant obstacles remain. Vibratory modes can exhibit subcycles involving all three fracture modes, particularly when neighboring vibratory modes are active simultaneously. Inevitably, a real-world application of the method will require a fully 3D pairing method, which remains to be defined.

18

Also, evidence from other authors [21,27] suggests that addition of shear modes into an otherwise mode I dominated cycle can in fact slow or arrest the crack in some regimes, as opposed to speeding it up as would be predicted with positive fracture mode asymmetry ratios. Further, Tschegg [20] showed that cracks propagating (planar) in pure mode III can slow down and arrest even when the applied ΔK_{III} increases with crack length. As aluded to earlier, these shortcomings are likely attributable to roughness induced closure associated with shear mode growth, which is not correctly accounted for by the simple mode I plasticity induced closure/friction method presented herein. It is nevertheless hoped that the framework provided will remain useful as further advances remedy these deficiencies.

References
[1] Need appropriate reference
[2] P. A. Wawrzynek, A. R. Ingraffea, "Interactive Finite-Element Analyses of Fracture Processes: An Integrated Approach", *Theoretical and Applied Fracture Mechanics*, Vol. 8, 1987, pp. 137-150.
[3] F. Erdogan, G. C. Sih; "On the Extension of Plates under Plane Loading and Transverse Shear", *Journal of Basic Engineering*, Vol. 85D, No. 4, pp. 519-527, 1963.
[4] A. Saito, M. Castanier, c. Pierre, O. Podou, "*Efficient Nonlinear Vibration Analysis of the Forced Response of Rotating Cracked Blades*", J. Comput.Nonlinear Dynam., Vol 4, Issue 1, Jan, 2009.
[5] A. Hoenig, "Near-Tip Behavior of a Crack in a Plane Anisotropic Elastic Body", *Engineering Fracture Mechanics*, Vol. 16, No. 3, pp. 3930403, 1982.
[6] G. P. Cherapanov, *Mechanics of Brittle Fracture*, McGraw-Hill, New York, 1979.
[7] B. E. Amstutz, M. A. Sutton, D. S. Dawicke, and J. C. Newman, "An Experimental Study of CTOD for Mode I/Mode II Stable Crack Growth in Thin 2024-T3 Aluminum Specimens", *Fracture Mechanics: 26th Volume*, ASTM STP 1256, American Society for Testing and Materials, pp. 257-271, 1995.
[8] N. Hallback, F. Nilsson, "Mixed-Mode I/II Fracture Behaviour of an Aluminium Alloy", *Journal of the Mechanics and Physics of Solids*, Vol. 42, No. 9, pp. 1345-1374, 1994.
[9] T. M. Maccagno, J. F. Knott, "The Fracture Behaviour of PMMA in Mixed Modes I and II", *Engineering Fracture Mechanics*, Vol. 34, No. 1, pp. 65-86, 1989.
[10] T. M. Maccagno, J. F. Knott, "The Low Temperature Brittle Fracture Behaviour of Steel in Mixed Modes I and II", *Engineering Fracture Mechanics*, Vol. 38, No. 2/3, pp. 111-128, 1991.

[11] Y. J. Chao, S. Liu, "On the Failure of Cracks Under Mixed-Mode Loads", *International Journal of Fracture*, Vol. 87, pp. 201-223, 1997.

[12] C. Dalle Donne, H. Doker, "Plane Stress Crack Resistance Curves of an Inclined Crack Under Biaxial Loading", *Multiaxial Fatigue and Deformation Testing Techniques*, ASTM STP 1280, American Society for Testing and Materials, pp. 243-263, 1997.

[13] A. P. Kfouri, M.W. Brown, "A Fracture Criterion for Cracks Under Mixed-Mode Loading", *Fatigue & Fracture Mechanics of Engineering Structures & Materials*, Vol. 18, No. 9, pp. 959-969, 1995.

[14] M. B. Buczek, C. T. Herakovitch, "A Normal Stress Criterion for Crack Extension Direction in Orthotropic Composite Materials", *J. Composite Materials*, Vol. 19, pp. 544-533, 1985.

[15] R. G. Pettit, *Crack Turning Integrally Stiffened Aircraft Structures*, PhD Dissertation, Cornell University, pp. 61-67, 2000.

[16] *High Cycle Fatigue (HCF) Life Assurance Methodologies*, Annual Technical Report., Contract No. RSC99009, delivered by Pratt & Whitney to University of Dayton Research Institute, pp. A-30 to A-50, 15 April, 2001.

[17] R. K. Kersey, D. P. DeLuca, R. G. Pettit, *Parametric Study of Fatigue Crack Threshold and HCF/LCF Interaction in Single Crystal Superalloy*, Aeromat 2003.

[18] J. C. Newman, Jr., "A Crack Opening Stress Equation for Fatigue Crack Growth", *Int. J. Fract*. 24, R131-R135 (1984).

[19] H. Nayeb-Hashemi, F. A. McClintock, R. O. Ritchie, "Effects of Friction and High Torque on Fatigue Crack Propagation in Mode III", *Metall. Transactions A*, Vol 13A, pp. 2197-2204, 1982.

[20] E. K. Tschegg, "Sliding Mode Crack Closure and Mode III Fatigue Crack Growth in Mild Steel", *Acta Metall*., Vol. 31, No. 9, pp. 1323-1330, 1983.

[21] J. P. Campbell, R. O. Ritchie, "Mixed Mode, High-cycle Fatigue-Crack Growth Thresholds in Ti 6-AL-4V", *Engineering Fracture Mechanics*, Vol. 67, pp. 209-249.

[22] NASGRO4 manual.   www.nasgro.com

[23] S.C. Forth et al, *Fatigue Fract Eng Mat Struct*, Vol. 25, pp. 3-15, 2002.

[24] T.J. Boone, P.A. Wawrzynek, A. R. Ingraffea, "Finite Element Modeling of Fracture Propagation in Orthotropic Materials, *Engineering Fracture Mechanics*, Vol. 26, No. 2, pp. 185-201, 1987.

[25] K. Tanaka et al, Fatigue Crack Propagation from a Precrack Under Combined Torsional and Axial Loading, *Fatigue & Fracture of Engng. Mater. Struct*., Vol 26, pp. 73-82, 2005.

[26] Highsmith, Shelby, PhD Dissertation. Georgia Institute of Technology, 2009.

[27] Feng et al, International Journal of Fatigue, Vol. 28, pp. 19-27, 2006